Mode-Matching Design of Substrate Mounted Waveguide (SMW) Components

Jan Schorer, *Graduate Student Member, IEEE*, Jens Bornemann, *Fellow, IEEE*, and Uwe Rosenberg, *Senior Member, IEEE*

***Abstract*— The mode-matching technique (MMT) is employed to analyze and design the transition from substrate integrated waveguides (SIWs) to substrate mounted waveguides (SMWs) that are mounted on top and/or at the bottom of the substrate. Coupling between the layers is facilitated by apertures of the thickness of the substrate's metallization. By appropriately segmenting the transition, a simple and fast MMT routine is developed. The results obtained for a single waveguide resonator mounted on the substrate agree well with simulations in CST and HFSS and, thus, validate the MMT code. Furthermore, the routine is extended to accommodate the design of more complex structures. A five-resonator SMW filter with additional SIW resonators to add transmission zeros and a diplexer are presented and prototyped. All the measured results are in good agreement with the MMT and the CST simulation results, thus validating the design procedure.**

***Index Terms*— Filters, mode-matching technique (MMT), substrate integrated waveguide (SIW), substrate mounted waveguide (SMW), waveguides.**

I. Introduction

SUBSTRATE integrated circuits provide a convenient opportunity for integration of previously bulky components in single- or multilayered substrate arrangements. Especially, substrate integrated waveguide (SIW) circuitry has been developed into a mature technology over the last decade [1].

In order to interface with surface-mounted active components, interconnects to other transmission line structures, such as microstrip or coplanar waveguide, are required [2]. To reduce the relatively high losses in microstrip filters operating in the higher gigahertz range, a substrate mounted waveguide (SMW) principle has been introduced [3]. A Ka-band prototype demonstrates lower insertion loss and better electrical performance that could not be obtained with a planar microstrip filter structure [4]. Due to the fact that SIW filter and diplexer technologies suffer from relatively high insertion losses, the SMW principle lends itself to applications in SIW. It contributes to the effort to overcome a major bottleneck of SIW technology, namely, high occurring insertion loss, while maintaining a fully shielded electromagnetic environment and a high degree of integration together with the advantage of low cost, high volume, production.

Therefore, this paper first focuses on several aspects for the design of SMW components. A mode-matching technique (MMT) approach to design an SIW-to-SMW transition is presented, and the MMT approach is extended to develop a routine for the full-wave design of coupled SMW waveguide filters. These two topics have been addressed in [5] and [6], respectively, where the approach is successfully used to design the first coupled resonator SMW-on-SIW filter [6].

In addition to [5] and [6], the MMT is now extended to accommodate a combination of SMW and SIW resonators in order to create transmission zeros. Moreover, a new MMT model is developed to divert the SIW input signal into two different SMW components situated in different layers. Based on this model, an SMW diplexer with channel filters on top and bottom of the SIW substrate is designed and prototyped. All extensions of the MMT model are validated by simulations in commercially available field solvers and by measurements. The overall MMT model will aid in the full-wave design of low-loss SMW waveguide filters and diplexers and, thus, contribute to the solution of a bottleneck in SIW technology. Moreover, it is expected that in an industrial fabrication process, SMW parts will be precisely picked and placed on the printed circuit board together with all other components prior to passing a reflow solder process.

This paper is organized as follows. Section II presents the adaption of the MMT to SIW-to-SMW transitions for three different variations and highlights the filter design process. Section III provides manufacturing details and dimensions of filter and diplexer prototypes. Section IV presents theoretical and experimental results, and Section V summarizes our findings.

II. Theory

A. SIW-to-SMW Transition

Fig. 1 shows the side view of an SIW-to-SMW transition. The SIW is coupled to the SMW by an aperture in the top metallization of the substrate. At a certain distance after the aperture, the SIW is shorted using a row of via holes. In the waveguide, the fundamental TE_{10} mode is excited, and

Manuscript received October 15, 2015; revised January 27, 2016; accepted June 3, 2016. Date of publication July 7, 2016; date of current version August 4, 2016. This work was supported by the TELUS Grant in Wireless Communications. An earlier version of this paper was presented at the 2015 IEEE MTT-S International Conference on Numerical Electromagnetic and Multiphysics Modeling and Optimization (NEMO 2015), Ottawa, ON, Canada, August 2015.

J. Schorer was with the Department of Electrical and Computer Engineering, University of Victoria, Victoria, BC V8W 3P6, Canada. He is now with Airbus Defence and Space, Ulm 89077, Germany (e-mail: schorerj@uvic.ca).

J. Bornemann is with the Department of Electrical and Computer Engineering, University of Victoria, Victoria, BC V8W 3P6, Canada (e-mail: j.bornemann@ieee.org).

U. Rosenberg is with Mician Global Engineering GbR, Bremen 28195, Germany (e-mail: uwe.rosenberg@ieee.org).

Color versions of one or more of the figures in this paper are available online at http://ieeexplore.ieee.org.

Digital Object Identifier 10.1109/TMTT.2016.2582484

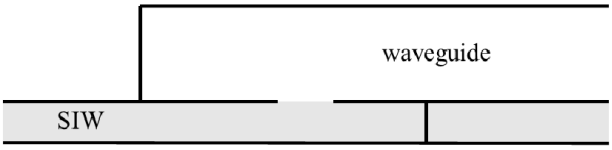

Fig. 1. Side view of the transition between SIW and SMW.

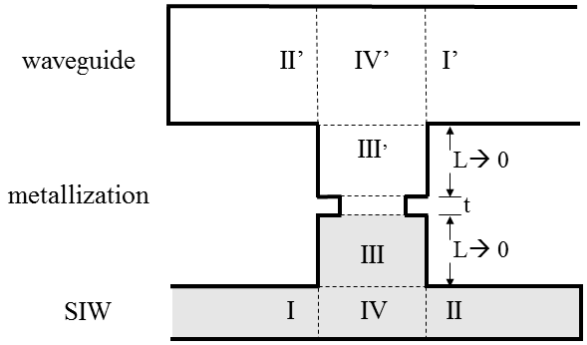

Fig. 2. Segmentation of the SIW-to-SMW transition for MMT analysis.

the distance to the short is adjusted to improve transmission performance.

The segmentation used in the MMT is shown in Fig. 2 and involves discontinuities in all three directions. Note that the subsections are either homogeneously filled with the dielectric material of the substrate (or with air) or are entirely transverse to the discontinuities. Therefore, a full set of TE_{mn} and TM_{mn} modes must be considered, but the inclusion of hybrid modes is avoided.

Following the general MMT procedure [7], the transverse electric and magnetic fields in regions I and II at their respective boundaries with region IV are given as

$$\begin{aligned}\vec{E}_T^{\mathrm{I}}(z=0) &= \sum_q \sqrt{Z_{hq}^{\mathrm{I}}}\left(\nabla T_{hq}^{\mathrm{I}} \times \vec{e}_z\right)\left[F_{hq}^{\mathrm{I}} + B_{hq}^{\mathrm{I}}\right] \\ &\quad - \sum_p \sqrt{Z_{ep}^{\mathrm{I}}}\left(\nabla T_{ep}^{\mathrm{I}}\right)\left[F_{ep}^{\mathrm{I}} + B_{ep}^{\mathrm{I}}\right] \\ &= \vec{E}_T^{\mathrm{II}}(z=c) \\ \vec{H}_T^{\mathrm{I}}(z=0) &= \sum_q \sqrt{Y_{hq}^{\mathrm{I}}}\left(\nabla T_{hq}^{\mathrm{I}}\right)\left[F_{hq}^{\mathrm{I}} - B_{hq}^{\mathrm{I}}\right] \\ &\quad + \sum_p \sqrt{Z_{ep}^{\mathrm{I}}}\left(\nabla T_{ep}^{\mathrm{I}} \times \vec{e}_z\right)\left[F_{ep}^{\mathrm{I}} - B_{ep}^{\mathrm{I}}\right] \\ &= \vec{H}_T^{\mathrm{II}}(z=c) \end{aligned} \tag{1}$$

where q and p are the mode indices defining the cross-section functions as

$$\begin{aligned} T_{hq\to m,n}^{\mathrm{I}} &= A_q^{\mathrm{I}} \frac{\cos\left(\frac{m\pi}{a}x\right)}{\sqrt{1+\delta_{0m}}} \frac{\cos\left(\frac{n\pi}{b}y\right)}{\sqrt{1+\delta_{0n}}} = T_{hq}^{\mathrm{II}} \\ T_{ep\to m,n}^{\mathrm{I}} &= D_P^{\mathrm{I}} \sin\left(\frac{m\pi}{a}x\right) \sin\left(\frac{n\pi}{b}y\right) = T_{ep}^{\mathrm{II}} \end{aligned} \tag{2}$$

where A and D are the normalization terms and δ is the Kronecker delta. Parameter a in (2) denotes the equivalent SIW width [8]. F and B in (1) are forward and backward propagating (or evanescent) wave amplitudes. The wave impedances and admittances are given as

$$\begin{aligned} Z_{hq\to m,n}^{\mathrm{I}} &= \frac{1}{Y_{hq}^{\mathrm{I}}} = \frac{\omega\mu_0}{\sqrt{k_0^2\varepsilon_r - \left(\frac{m\pi}{a}\right)^2 - \left(\frac{n\pi}{b}\right)^2}} \\ Y_{ep\to m,n}^{\mathrm{I}} &= \frac{1}{Z_{ep}^{\mathrm{I}}} = \frac{\omega\varepsilon_0\varepsilon_r}{\sqrt{k_0^2\varepsilon_r - \left(\frac{m\pi}{a}\right)^2 - \left(\frac{n\pi}{b}\right)^2}}. \end{aligned} \tag{3}$$

The respective fields and quantities of region III at its boundary region IV are

$$\begin{aligned} \vec{E}_T^{\mathrm{III}}(y=b) &= \sum_r \sqrt{Z_{hr}^{\mathrm{III}}}\left(\nabla T_{hr}^{\mathrm{III}} \times \vec{e}_y\right)\left[F_{hr}^{\mathrm{III}} + B_{hr}^{\mathrm{III}}\right] \\ &\quad - \sum_s \sqrt{Z_{es}^{\mathrm{III}}}\left(\nabla T_{es}^{\mathrm{III}}\right)\left[F_{es}^{\mathrm{III}} + B_{es}^{\mathrm{III}}\right] \\ \vec{H}_T^{\mathrm{III}}(y=b) &= \sum_r \sqrt{Y_{hr}^{\mathrm{III}}}\left(\nabla T_{hr}^{\mathrm{III}}\right)\left[F_{hr}^{\mathrm{III}} - B_{hr}^{\mathrm{III}}\right] \\ &\quad + \sum_s \sqrt{Y_{es}^{\mathrm{III}}}\left(\nabla T_{es}^{\mathrm{III}} \times \vec{e}_y\right)\left[F_{es}^{\mathrm{III}} - B_{es}^{\mathrm{III}}\right] \end{aligned} \tag{4}$$

$$\begin{aligned} T_{hr\to i,k}^{\mathrm{III}} &= A_r^{\mathrm{III}} \frac{\cos\left(\frac{i\pi}{a}x\right)}{\sqrt{1+\delta_{0i}}} \frac{\cos\left(\frac{k\pi}{c}z\right)}{\sqrt{1+\delta_{0k}}} \\ T_{es\to m,n}^{\mathrm{III}} &= D_S^{\mathrm{III}} \sin\left(\frac{i\pi}{a}x\right) \sin\left(\frac{k\pi}{c}z\right) \end{aligned} \tag{5}$$

$$\begin{aligned} Z_{hr\to i,k}^{\mathrm{III}} &= \frac{1}{Y_{hr}^{\mathrm{III}}} = \frac{\omega\mu_0}{\sqrt{k_0^2\varepsilon_r - \left(\frac{i\pi}{a}\right)^2 - \left(\frac{k\pi}{c}\right)^2}} \\ Y_{es\to i,k}^{\mathrm{III}} &= \frac{1}{Z_{es}^{\mathrm{III}}} = \frac{\omega\varepsilon_0\varepsilon_r}{\sqrt{k_0^2\varepsilon_r - \left(\frac{i\pi}{a}\right)^2 - \left(\frac{k\pi}{c}\right)^2}}. \end{aligned} \tag{6}$$

The fields and quantities in region IV are taken as a superposition of those in regions I–III. Then the generalized (modal) scattering matrix of the three ports is obtained as follows. First, the transverse electric fields are matched at the boundaries with the respective other two ports shorted. This results in expressions for the wave amplitudes in region IV. Second, matching the transverse magnetic fields yields the overall scattering matrix of the junction. The reader is referred to [7] and [9] for details. The short at the end of region II is incorporated using its input reflection coefficient at $z = c$ (Fig. 2)

$$\Gamma = \mathrm{Diag}\left\{-\exp\left(-j2k_{zq,p}^{\mathrm{II}}L_s\right)\right\} \tag{7}$$

where k_z represents the propagation constants in region II and L_s is the distance between $z = c$ and the short. Assuming that the generalized scattering parameter submatrices of the junction are denoted by S_{ik} $(i, k = 1, 2, \text{ and } 3)$, then the two-port submatrices between ports I and III are

$$\begin{aligned} S_{11}^{2p} &= S_{11} + S_{12}WS_{21} \quad S_{13}^{2p} = S_{13} + S_{12}WS_{23} = S_{31}^{2pT} \\ S_{31}^{2p} &= S_{31} + S_{32}WS_{23} = S_{13}^{2pT} \quad S_{33}^{2p} = S_{33} + S_{32}WS_{23} \end{aligned} \tag{8}$$

where $W = \Gamma(I - S_{22}\Gamma)^{-1}$, I is the unity matrix, and T denotes transposed.

Once this procedure is established, it can also be used to analyze the shorted waveguide junction between ports I' and II' (Fig. 2) by changing the dimensions and material constants accordingly.

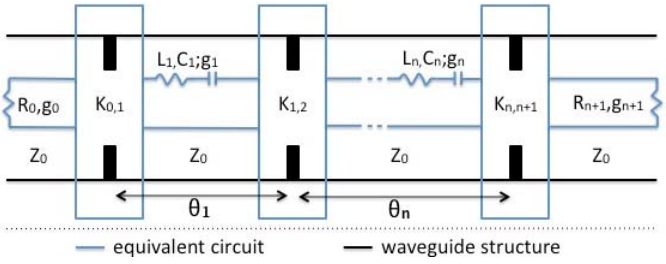

Fig. 3. Equivalent circuit model for direct-coupled resonator filters.

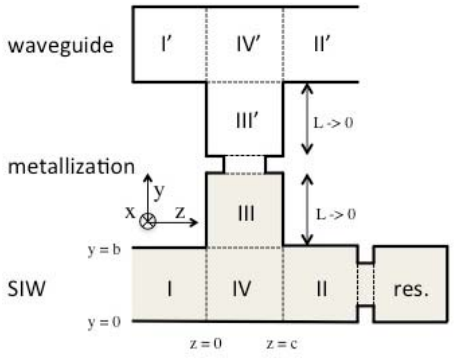

Fig. 4. Segmentation for the combination of SIW and SMW resonators.

Finally, the aperture of metallization thickness t is considered by a discontinuity that includes not only the aperture size but also a change in waveguide width as for the same frequency band, the waveguide is usually wider than the SIW due to the lack of substrate material.

The S matrix representation of the transition in Fig. 2 allows a straightforward link to theoretical filter synthesis [10]. By specifying the filter function and topology, e.g., Chebychev for direct-coupled resonator filters, impedance inverter values for different MMT segments can be synthesized based on their S matrices. Fig. 3 relates the equivalent circuit model to the waveguide discontinuities for this topology.

These impedance inverter values, denoted by $K_{n,n+1}$ in Fig. 3, can be matched to theoretical values obtained from standard filter synthesis procedures by applying, e.g., Chebychev polynomials. Note that the iris in Fig. 2 acts as the first inverter of an SMW filter. The dimensions of the coupling irises are obtained by a 1-D optimization routine varying the apertures of the irises. Finally, the lengths of the resonators separating the irises are calculated utilizing the inverter phases θ_n (Fig. 3). More waveguide apertures and resonators can be added and designed by standard MMT procedures [7].

B. Combination of SIW and SMW Resonators

For the combination of SIW and SMW resonators, a resonator realized in SIW technology is attached to the SIW T-junction as shown in Fig. 4. This combination with SMW resonators on top of the substrate represents a filter with an added transmission zero (providing a so-called notch in the combined transmission response); alternatively, it can be considered as an extracted pole in an overall filter design.

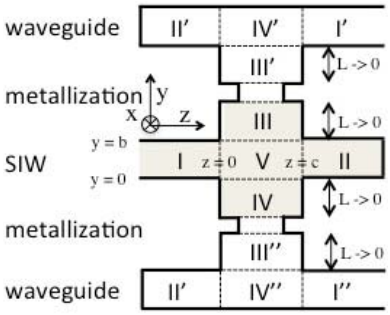

Fig. 5. Segmentation for the double-layer SIW-to-SMW transition.

The resulting transmission zero is used to enhance the steepness of the filter skirts, thus providing improved selectivity. The SIW resonator is fed via an H-plane iris also calculated with the MMT. Looking at the segmentation of this transition model (Fig. 4), the electromagnetic calculation procedure follows the MMT introduced above. First, the superposition of region IV is calculated, and then different from the calculation of the previous transition from SIW to SMW, the SIW T-junction is not short circuited by a waveguide stub at region II, but two pieces of SIW separated by the H-plane iris are added. This configuration represents another impedance inverter in itself, thus allowing the design of this transition toward the theoretical impedance inverter value.

The numerical implementation follows (1)–(8), except that (7) is replaced by

$$\Gamma = S^i_{11} - S^i_{12}\left(I + S^i_{22}\right)S^i_{21} \tag{9}$$

where S^i is the modal scattering matrix of the SIW iris including the length of section II (Fig. 4), the iris, and the length of the resonator.

C. Double Layer SIW-to-SMW Transition

A double-layer transition becomes necessary when constructing SMW filter structures with two different branches to efficiently utilize available substrate surface space. A possible segmentation, chosen later as a diplexer circuit, is depicted in Fig. 5. The SIW layer is now realized as a four-port junction. Region I is the input, region II is a shortened SIW stub, and regions III and IV are the outputs feeding the SMW resonators via separate irises. As previously, rectangular slots in the top and bottom metallization of the SIW act as iris inverters with discontinuities in the E- and H-plane. Region V is calculated as a superposition using the respective fields and quantities established for each region, I–IV (similar to Section II-A). Let S_{ik} (i, k =1, 2, 3, and 4) be the modal scattering matrix of the four-port junction, then, by shortening region II at a distance L_s (7), the three-port scattering matrix is established as

$$\begin{aligned} S^{3p}_{11} &= S_{11} + S_{12}WS_{21} \quad S^{3p}_{13} = S_{13} + S_{12}WS_{23} = S^{3pT}_{31} \\ S^{3p}_{14} &= S_{14} + S_{12}WS_{24} = S^{3pT}_{41} \quad S^{3p}_{33} = S_{33} + S_{32}WS_{23} \\ S^{3p}_{34} &= S_{34} + S_{32}WS_{24} = S^{3pT}_{43} \quad S^{3p}_{44} = S_{44} + S_{42}WS_{24} \end{aligned} \tag{10}$$

with Γ and W as in (7) and (8), respectively. Then adjacent double-step irises in the top and bottom metallization are implemented.

From this point on, the procedure is similar to the single transition of Section II-A. Both parameters are cascaded with a shortened conventional waveguide T-junction leading to an overall three-port structure. The modal scattering matrix representation of the entire system shown in Fig. 5 is then used to calculate the impedance inverter values for the two transitions. By implementing a 2-D optimization routine, it is possible to match the impedance inverter values to the theoretical values from filter synthesis. This method can also be used to design multiport networks. Each transition is treated as a starting point for one of two possible branches of the architecture, which then can be extended in an arbitrary SMW topology on the top or the bottom of the SIW.

III. Prototypes

In addition to the Chebychev design of [6], which will not be repeated here, the design routines established above are applied to prototype two SMW circuits:

1) a coupled five-resonator SMW filter combined with two SIW cavity resonators according Section II-B to introduce two transmission zeros;
2) a diplexer according to Section II-C utilizing the transition from SIW to two SMW layers feeding the two branches.

Note that in Design 1, the SIW cavities are added only to improve the near-band rejection of the existing SMW filter [6] with additional transmission zeros. It is not an extracted-pole filter, because an extracted-pole filter with seven poles would require an overall design with the SMW component to be reprototyped.

Both prototypes are designed for K-band applications. The via hole radius is 0.65 mm, and the pitch of the vias is 1 mm. The initial MMT design is fine optimized to accommodate production restrictions using CST. This adjustment includes the introduction of the corner radius for the SMW parts of 1.5 mm. The prototypes are designed on a Rogers Duroid/RT 6002 substrate with a permittivity of 2.94. Design 1 is realized in a sandwich construction with the following different layers: the substrate, a copper 101 sheet (height of the resonators) with the resonator contour cut into it, and another copper sheet acting as lid to the structure. Wire electrical discharge machining is used to manufacture the SMW resonators. It provides an accuracy of up to 1–2 μm. For the SMW-SIW resonator combination filter, another metal sheet is placed below the structure to provide even pressure after assembly.

For the diplexer (Design 2), the sandwich construction structure is mirrored on the bottom of the substrate. The alignment between the different layers is realized using stainless steel pins. The pressure to hold the structure together is applied with screws and nuts. A tolerance analysis, carried out in [6], has revealed ± 25 μm as an acceptable margin for alignment. The conductivity between the different layers is ensured using a conductive silver paste. Based on [6], the accuracy acceptable for the SMW parts is ± 10 μm.

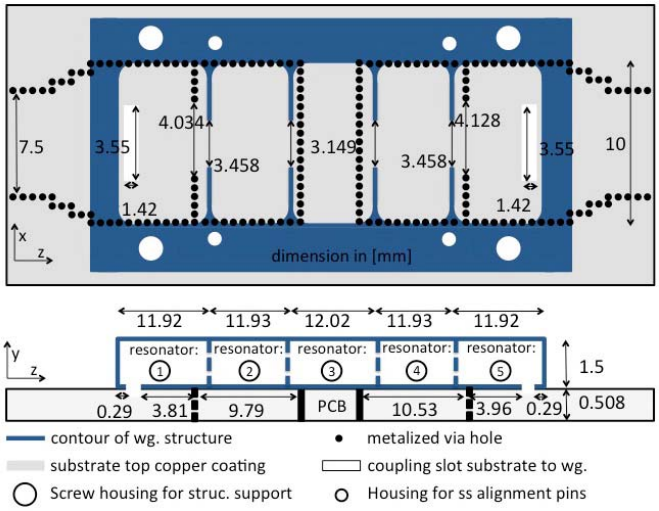

Fig. 6. Top and side views of the coupled five-resonator SMW filter with additional SIW resonators (Design 1). All dimensions are in millimeters.

In comparison, the tolerances of the SIW part have been shown to be the least sensitive dimensions; this has also been reported in [11].

Both prototypes are designed with a transformer at the SIW input port. These transformers permit the use of less restrictive iris dimensions, hence less sensitivity of the transition, thus enhancing the overall robustness of the prototype design. In the combined SIW-SMW filter (Design 1), the SIW resonators are used to place transmission zeros on either side of the filter passband. The exact resonant frequency is determined by adjusting the SIW iris width and resonator length in the MMT routine.

A sketch of Design 1 prototype including the dimensions is presented in Fig. 6. It shows the SMW part consisting of the contour and the lid on the top and the bottom of the PCB.

In Fig. 7, a schematic of the second prototype (Design 2) and its dimensions are displayed. The double-layer junction has been fine optimized using CST Microwave Studio to compensate for the loading effect of the two branches. This was not taken into account during the initial design. Compared with Design 1, it is necessary to rotate the iris for the second transition (SMW to SIW) due to space limitations of the substrate caused by the SIW output ports. The transition is designed with the MMT by adjusting the integral limits for the mode matching of the fields. Using the transformer together with an iris length oriented in the longitudinal z-direction causes unwanted higher order resonances in the transformer. Therefore, the transformer is removed from the final design, which causes a slight increase in sensitivity of the output iris. In addition, the SIW fabrication process requires a 200-μm distance for the iris in the z and x directions in reference to the via holes. This margin is introduced to avoid deburring at the edges of the via holes during the PCB process.

IV. Results

In order to verify the MMT code based on the theory presented in Section II, an SIW-to-SMW transition is designed for operation in the 19-GHz range. A single TE_{10}-mode resonator

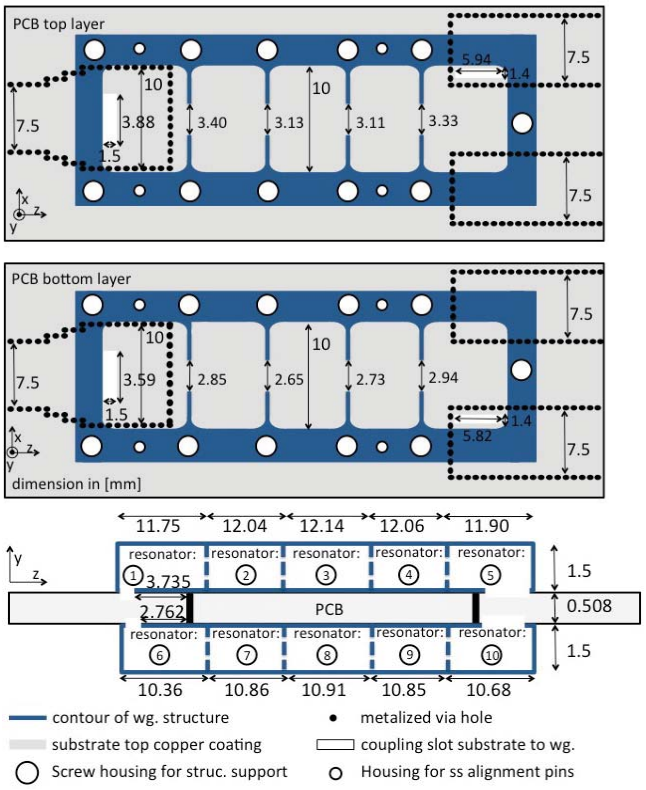

Fig. 7. Top and side views of the double-layer SMW diplexer (Design 2). All dimensions are in millimeters.

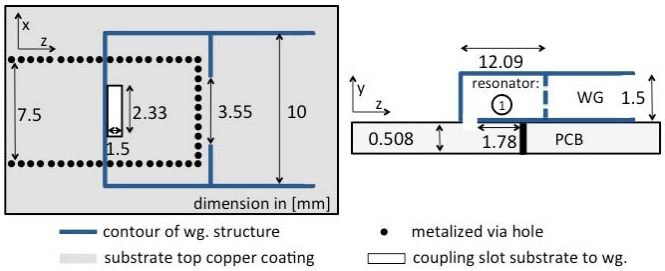

Fig. 8. Top and side views of the SIW-to-SMW transition with additional waveguide TE_{10}-mode resonator.

is added to the top waveguide to create significant frequency sensitivity. Fig. 8 shows the top and side views of the structure, clearly identifying the different layers, the coupling aperture, the resonator, and the via holes in the SIW. For given SIW and waveguide widths, the initial aperture size, which acts as inverter to the waveguide resonator, is determined by filter theory (see above), e.g., [10]. The final values as well as the exact positions of the SIW and waveguide shorts are determined by fine optimization within the MMT.

Fig. 9 shows the results obtained by the MMT and compares them with simulations in CST and HFSS. Very good agreement is observed in general. The only discrepancy appears to be a very slight frequency shift of 18 MHz, which amounts to less than 0.1% at 19 GHz. The deviation is attributed to the fact that CST and HFSS simulate the actual via holes and the initial transition to an all-dielectric filled waveguide. The MMT routine considers only the equivalent waveguide width of the SIW [8] in view of a simple and fast implementation.

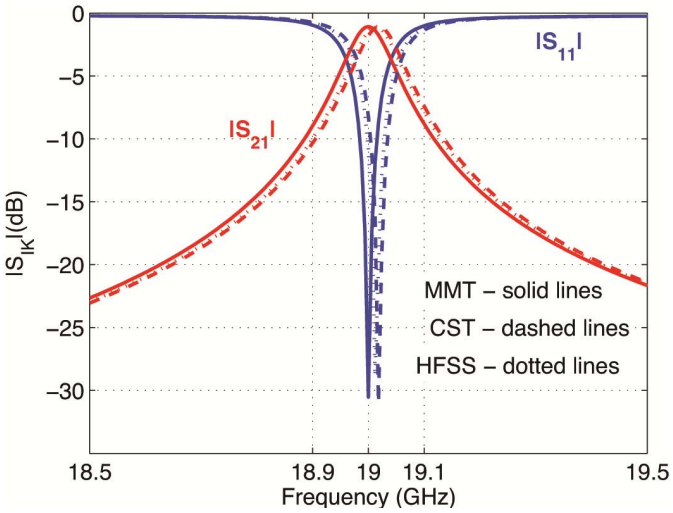

Fig. 9. Comparison of the results obtained by the MMT with simulations in CST and HFSS.

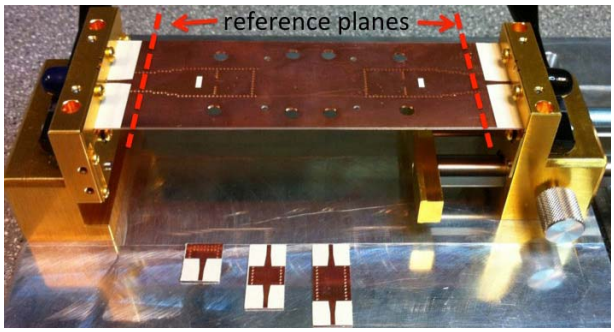

Fig. 10. Design 1 (substrate part only) in the test fixture and calibration standards (short, through and line).

The initial tests have shown that depending on implementation, the MMT code is at least one order of magnitude faster than CST and HFSS. Thus, the extremely small deviation is acceptable in view of a timelier optimization and design process of SMW components. Note that the advantage of the MMT over general field solvers is expected to increase with more complex SMW structures. However, this holds only for structures suiting a proper segmentation and boundaries that fall along the unit vectors of the coordinate system.

For measurement purposes of Designs 1 and 2, microstrip transitions are designed to feed all SIW ports. Such transitions are de-embedded by performing a TLR calibration of the vector network analyzer (VNA). The calibration standards (Fig. 10) required for this procedure are custom made, placing the measurement reference planes (the red dashed lines in Fig. 10) at the beginning of the SIW shown in Figs. 6 and 7.

Fig. 11 shows the manufactured prototype components of the filter (Design 1). The bottom part shows the SIW with the coupling slots and microstrip transitions at opposite sides.

Fig. 12 presents a comparison between the simulated and measured results of the SMW filter with two SIW resonators (Design 1). In addition, measurements of a directly coupled five-resonator filter without SIW resonators, as presented in [6], are included for comparison [Fig. 12(a)].

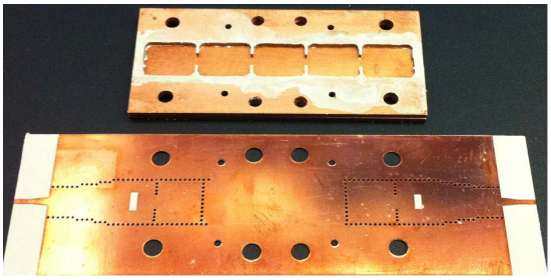

Fig. 11. View of the manufactured prototype (Design 1) with SMW sandwich part (top) and SIW (bottom).

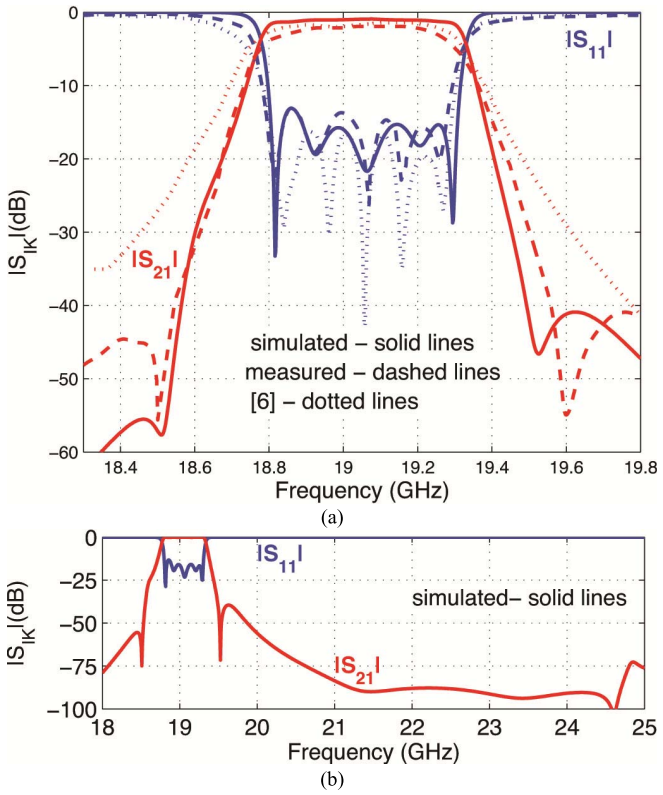

Fig. 12. Design 1: comparison of the results obtained by the MMT/CST with prototype measurement data. (a) Narrowband. (b) Wideband.

For the S_{11} parameter, good agreement between simulations and measurement is obtained. A marginal wider bandwidth in the measurement is observed, resulting in a slightly smaller rejection increase at the filter's cut-off frequencies, especially visible at the lower one. This is caused by the vertical alignment accuracy of the sandwich construction (see [6]). Reflection zeros are observed at identical frequencies for the lower passband, slightly increasingly deviating between measurement and simulation toward the upper passband. The magnitude of the ripples in the passband is a bit higher for the measured data, but well within the expected measurement accuracy regarding the sandwich construction.

As for S_{21}, the simulated and measured data in the passband deviate by 1–2 dB. This is mostly due to higher conductor losses caused by the connectivity between the sandwiched layers and possible oxidation of the prototypes' surfaces. For the transmission zeros caused by the SIW resonators, a small shift in frequency between simulation and measurement is observed. The zero at the higher frequency deviates by approximately 100 MHz. Nevertheless, both transmission zeros are well developed, demonstrating the intended use to obtain extra notches and thus improving the selectivity of the existing five-pole filter. This is clearly shown when the measurement of this component (Design A) is compared with that of the directly coupled five-resonator filter without SIW resonators as presented in [6]. The measured insertion loss levels of the two filters deviate by about 1 dB. The simulation data do not imply different Q values for the single SMW resonators. Therefore, this discrepancy is attributed to measurement inaccuracy.

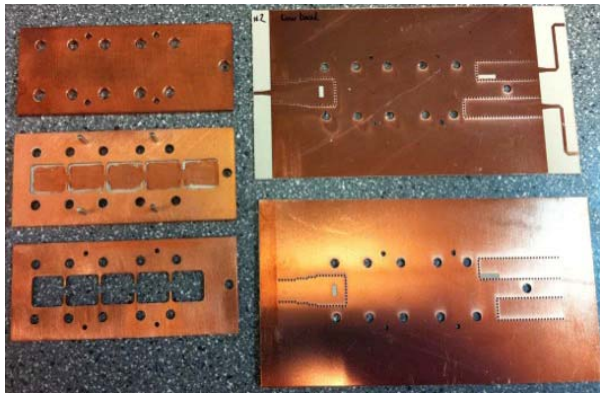

Fig. 13. View of the manufactured diplexer prototype. Left: SMW sandwich parts. Right: top and bottom view of SIW.

Fig. 12(b) shows a wideband simulation confirming that there are no spurious unwanted resonances over the rest of the K-band.

Fig. 13 shows the manufactured prototype of the diplexer (Design 2) in a disassembled state. Since two SIW circuits have been fabricated, their top and bottom views are shown in Fig. 13 (right). The two SMW filters [Fig. 13 (left)] are mounted on the top and bottom metallization as shown in Fig. 7.

A comparison between the measured and simulated results is displayed in Fig. 14(a). In general, good agreement between simulation and measurement is observed with a distinct separation between the two frequency bands. A deviation between the computed and measured selectivity is observed at rejection levels below 40 dB. This is attributed to the obtainable accuracy using calibration standards to deembed the coax-to-microstrip-to-SIW transitions. After calibration, a measurement of the line calibration standard revealed a $|S_{11}|$ value between -40 and -45 dB (not shown here), which can be taken as the minimum level of measurement accuracy. Similar discrepancies below -40 dB are observed for the T-junction SIW diplexer in [12].

As for the S_{11} parameter, the measured passbands are slightly wider than those obtained from the simulation. The steepness of the lower skirt selectivity of the upper band almost matches the simulation data. The other skirts are slightly off, where the widening of the lower frequency band is more pronounced than that of the upper one. The slight deviations in the positions of the reflection zeros are already known from the tolerance analyses presented in [6].

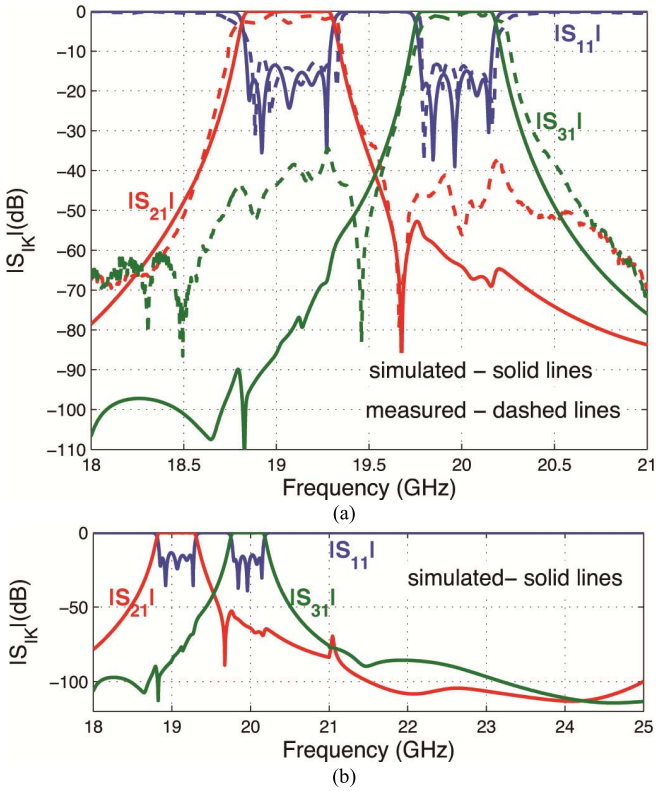

Fig. 14. Design 2: comparison of the results obtained by the MMT/CST with prototype measurement data. (a) Narrowband. (b) Wideband.

Therefore, they are attributed to manufacturing inaccuracies. The return loss ripples are marginally higher, about 2–3 dB, for the measured data, and are well within the expected deviation.

The same widening in bandwidth is observed in the measurements of the two passband transmission parameters S_{21} and S_{31}. The magnitude level falls about 1–2 dB short of the simulation. This was already observed in the previous prototype (Design 1) and is likely caused by the introduction of losses due to connectivity issues and surface oxidation. Therefore, the expected Q values of the prototyped diplexer and Design 1 are within the range of those presented in [6]. A ripple in the passband for the S_{21} and S_{31} insertion loss parameters is observed. These ripples can be attributed to measurement and calibration inaccuracies. These are likely caused by the movement of cables and the test fixture while switching from the calibration standards to the DUT. Other measurement inaccuracies are related to issues caused by the termination of the third unused port when measuring with a two-port VNA.

Fig. 14(b) shows a wider section of the K-band. This simulated data demonstrate that the diplexer does not exhibit any other spurious resonances. The current design successfully suppresses all signals in the rest of the K-band.

Focusing on insertion loss, SMW technology provides a significant improvement when compared with similar pure SIW circuits. For example, a filter similar to Design 1 (Fig. 6), but without the additional SIW resonators, exhibits a Q value that is roughly four times higher than the one of a comparable SIW filter [13].

V. Conclusion

An MMT for the analysis and design of SMW components on SIW technology is presented. The method is rigorous and includes the metallization thickness of the aperture. The specific segmentation of discontinuities in the MMT permits the use of regular waveguide TE_{mn} and TM_{mn} modes. The results obtained for a single resonant structure, which consists of the SIW-to-SMW transition and an added waveguide TE_{10}-mode cavity, shows very good agreement with CST and HFSS simulations. Furthermore, the results for the combination of SIW and SMW resonators demonstrate good agreement between MMT/CST and measurements, thus not only proving the validity of the MMT approach but also presenting a design for highly selective bandpass filters. The measured results of a more complex diplexer structure show good agreement with simulations obtained from MMT/CST. The MMT models presented here have proven to be valid and fast routines for the timely optimization and initial design of different SMW components. They facilitate an efficient way to design combined SIW–SMW, low-loss, passive, and frequency-selective systems.

References

[1] K. Wu, "State-of-the-art and future perspective of substrate integrated circuits (SICs)," in *Workshop Notes, IEEE MTT-S Int. Microw. Symp. Dig.*, Anaheim, CA, USA, May 2010, pp. 1–40.

[2] F. Taringou, J. Bornemann, and K. Wu, "Broadband coplanar-waveguide and microstrip low-noise amplifier hybrid integrations for K–band substrate integrated waveguide applications on low-permittivity substrate," *IET Microw., Antennas Propag.*, vol. 8, pp. 99–103, Jan. 2014.

[3] W. Menzel and M. Wetzel, "Waveguide filter integrated into a planar circuit," in *Proc. 32nd Eur. Microw. Conf.*, Milan, Italy, Sep. 2002, pp. 1–4.

[4] T. J. Müller, W. Grabherr, and B. Adelseck, "Surface-mountable metalized plastic waveguide filter suitable for high volume production," in *Proc. 33rd Eur. Microw. Conf.*, Munich, Germany, Oct. 2003, pp. 1255–1258.

[5] J. Schorer and J. Bornemann, "A mode-matching technique for the analysis of waveguide-on-substrate components," in *Proc. IEEE MTT-S Int. Conf. Numer. Electromagn. Multiphys. Modeling Optim. (NEMO)*, Ottawa, ON, Canada, Aug. 2015, pp. 1–3.

[6] J. Schorer, J. Bornemann, and U. Rosenberg, "Design of a surface mounted waveguide filter in substrate integrated waveguide technology," in *Proc. 45th Eur. Microw. Conf.*, Paris, France, Sep. 2015, pp. 757–760.

[7] J. Uher, J. Bornemann, and U. Rosenberg, *Waveguide Components for Antenna Feed Systems: Theory and CAD*. Norwood, MA, USA: Artech House, 1993.

[8] Z. Kordiboroujeni and J. Bornemann, "Designing the width of substrate integrated waveguide structures," *IEEE Microw. Wireless Compon. Lett.*, vol. 23, no. 10, pp. 518–520, Oct. 2013.

[9] E. Kühn, "A mode-matching method for solving field problems in waveguide and resonator circuits," *AEU-Int. J. Electron. Commun.*, vol. 27, pp. 511–518, Dec. 1973.

[10] G. Matthaei, L. Young, and E. M. T. Jones, *Microwave Filters, Impedance-Matching Networks, and Coupling Structures*, Dedham, MA, USA: Artech House, 1980.

[11] A. B. Alaya, M. Bozzi, L. Perregrini, N. Raveu, and K. Wu, "Comparison of fabrication tolerance sensitivity between substrate integrated waveguide and microstrip circuits," in *IEEE MTT-S Int. Microw. Symp. Dig.*, Phoenix, AZ, USA, May 2015, pp. 1–3.

[12] Z. Kordiboroujeni, J. Bornemann, and T. Sieverding, "K-band substrate integrated waveguide T-junction diplexer design by mode-matching techniques," in *Proc. Asia–Pacific Microw. Conf.*, Sendai, Japan, Nov. 2014, pp. 1297–1299.

[13] J. Schorer, J. Bornemann, and U. Rosenberg, "Comparison of surface mounted high quality filters for combination of substrate integrated and waveguide technology," in *Proc. Asia–Pacific Microw. Conf.*, Sendai, Japan, Nov. 2014, pp. 929–931.

Jan Schorer (GSM'14) received the bachelor's degree in electrical engineering and information technology and the master's degree in electrical engineering from the University of Applied Sciences Ravensburg–Weingarten, Weingarten, Germany, in 2010 and 2012, respectively, and the Ph.D. degree from the University of Victoria, Victoria, BC, Canada, in 2016.

He has been with the Computer-Aided Design of Microwave Integrated Circuits Group, Department of Electrical and Computer Engineering, University of Victoria, since 2011. Since April 2016, he has been with Airbus Defense and Space, Ulm, Germany.

Jens Bornemann (M'87–SM'90–F'02) received the Dipl.-Ing. and Dr.Ing. degrees in electrical engineering from the University of Bremen, Bremen, Germany, in 1980 and 1984, respectively.

He was a Consulting Engineer from 1984 to 1985. In 1985, he became an Assistant Professor with the University of Bremen. He has been with the Department of Electrical and Computer Engineering, University of Victoria, Victoria, BC, Canada, since 1988, where he became a Professor in 1992. He was a Fellow of the British Columbia Advanced Systems Institute, Vancouver, BC, Canada, from 1992 to 1995. In 1996, he was a Visiting Scientist with Spar Aerospace Limited, Ste-Anne-de-Bellevue, QC, Canada, and a Visiting Professor with the Microwave Department, University of Ulm, Ulm, Germany. He was a Co-Director of the Center for Advanced Materials and Related Technology with the University of Victoria from 1997 to 2002. He was a Visiting Professor with the Laboratory for Electromagnetic Fields and Microwave Electronics, ETH Zurich, Zurich, Switzerland, in 2003. He co-authored *Waveguide Components for Antenna Feed Systems: Theory and Design* (Artech House, 1993) and has authored/co-authored over 300 technical papers. His current research interests include radio frequency/wireless/microwave/millimeter-wave components and systems design, and field-theory-based modeling of integrated circuits, feed networks, and antennas.

Dr. Bornemann is a Fellow of the Canadian Academy of Engineering and a member of the European Microwave Association. From 1999 to 2002, he served as an Associate Editor of the IEEE TRANSACTIONS ON MICROWAVE THEORY AND TECHNIQUES in the area of microwave modeling and CAD. He served on the Technical Program Committee of the IEEE MTT-S International Microwave Symposium from 1999 to 2009. He was an Associate Editor of the *International Journal of Electronics and Communications* from 2006 to 2008. He serves on the Editorial Advisory Board of the *International Journal of Numerical Modeling*. He is a Registered Professional Engineer in the Province of British Columbia, Canada.

Uwe Rosenberg (M'89–SM'93) received the Dipl.-Ing. degree (Hons.) in electrical engineering (with a minor in telecommunication technique) from the Fachhochschule der Deutschen Bundespost, Dieburg, Germany, in 1982.

He was with Hydro Therm, Dieburg, Germany, from 1982 to 1983, where he was involved in the design and development of automatic safety and heating control circuits. He was with the Technische Hochschule Darmstadt, Darmstadt, Germany, from 1983 to 1985, where he was involved in the design and development of experimental installations and software components for microcomputer control systems. He joined the Space Division, Tesat-Spacecom GmbH & Company KG, Backnang, Germany, in 1985, where he was involved in the research and development of microwave filters, multiplexers, and passive subsystems for communications satellites. From 1989 to 2008, he was the Head of the Research and Development Laboratory for Passive Microwave Components and Subsystems with Ericsson GmbH, Backnang (which was, until December 2005, Marconi Communications GmbH and formerly Bosch Telecom GmbH, a Public Networks Division). During this period, he was in charge of research and development of integrated waveguide transceiver circuitries, channel branching networks (multiplexers), antenna feed and waveguide (feeder) systems for trunk and access radio applications, mobile base stations, large earth stations, and defense and communications satellites. He was appointed as a Manager of the Antenna Development Team from 2006 to 2008. In 2002, he started his own project and consultancy work for international companies with the design of novel passive microwave designs and subsystems for a variety of applications (earth stations, satellites, millimeter-wave communications equipment, mobile, and defense) providing design, measurement, production, and technology support and advice. He has been the Managing Director of Mician Global Engineering GbR, Bremen, Germany, since 2011, which he co-founded the same year together with partners. He co-authored *Waveguide Components for Antenna Feed Systems: Theory and CAD* (Artech House, 1993). He has also authored or co-authored over 100 technical papers and has originated more than 50 granted microwave design patents.

Mr. Rosenberg is a Member of the Verband der Elektrotechnik Elektronik Informationstechnik, the Informationstechnische Gesellschaft, and the Verein Deutscher Ingenieure. He is also a Member of the European Microwave Association and a Senior Member of the IEEE Microwave Theory and Techniques Society and the IEEE Antennas and Propagation Society.